2018-06-01

# Dunes on Pluto

Telfer, Matt



10.1126/science.aao2975
Science
American Association for the Advancement of Science (AAAS)

# Title: Dunes on Pluto

**Authors:** Matt W. Telfer[1*†], Eric J.R. Parteli[2†], Jani Radebaugh[3†], Ross A. Beyer[4,5], Tanguy Bertrand[6], François Forget[6], Francis Nimmo[7], Will M. Grundy[8], Jeffrey M. Moore[5], S. Alan Stern[9], John Spencer[9], Tod R. Lauer[10], Alissa M. Earle[11], Richard P. Binzel[11], Hal A. Weaver[12], Cathy B. Olkin[12], Leslie A. Young[9], Kimberley Ennico[5], Kirby Runyon[12], and The New Horizons Geology, Geophysics and Imaging Science Theme Team[‡]

**Affiliations:**

1. School of Geography, Earth and Environmental Sciences, Plymouth University, Drake Circus, Plymouth, Devon, UK, PL4 8AA.

2. Department of Geosciences, University of Cologne, Pohligstraße 3, 50969 Cologne, Germany.

3. Department of Geological Sciences, College of Physical and Mathematical Sciences, Brigham Young University, Provo, Utah, UT 84602, USA.

4. Sagan Center at the SETI Institute, Mountain View, CA 94043, USA.

5. NASA Ames Research Center, Moffett Field, CA 94035, USA.

6. Laboratoire de Météorologie Dynamique, Université Pierre et Marie Curie, Paris, France.

7. University of California Santa Cruz, Santa Cruz, CA, USA.

8. Lowell Observatory, Flagstaff, AZ, USA.

9. Southwest Research Institute, Boulder, CO, USA.

10. National Optical Astronomy Observatory, Tucson, AZ 85726, USA.

11. Department of Earth, Atmosphere, and Planetary Science, Massachusetts Institute of Technology, Cambridge, MA 02139, USA.

12. Johns Hopkins University Applied Physics Laboratory, Laurel, MD, USA.

† These authors contributed equally to this work.

* Correspondence to: matt.telfer@plymouth.ac.uk

‡ The list of team members is provided in the supplementary material

**Abstract**: The surface of Pluto is more geologically diverse and dynamic than had been expected, but the role of its tenuous atmosphere in shaping the landscape remains unclear. We describe observations of regularly spaced, linear ridges from the New Horizons spacecraft whose morphology, distribution and orientation are consistent with being transverse dunes. These are located close to mountainous regions and are orthogonal to nearby wind streaks. We demonstrate that the wavelength of the dunes (~ 0.4 – 1 km) is best explained by the deposition of sand-sized (~200-~300 μm) particles of methane ice in moderate winds (<10 m $s^{-1}$). The undisturbed morphology of the dunes, and relationships with the underlying convective glacial ice, imply that the dunes have formed in the very recent geological past.

**One Sentence Summary:**

We describe dune-like landforms on Pluto, which likely result from granular solids affected by the wind regime at the margin of an icecap and mountains.

**Main Text:**

Dunes require a supply of particulate material on a surface and a fluid boundary layer to entrain the grains (i.e. wind, for dunes on a planet's surface). They have been identified in some surprising locations: Contrary to predictions (*1*), Saturn's moon Titan has a broad belt of linear dunes encircling its equatorial latitudes (*2*), and despite the lack of a persistent atmosphere, eolian landforms (i.e. those related to wind) have also been suggested to occur on comet 67P/Churyumov-Gerasimenko (*3*). On July 14 2015, NASA's New Horizons spacecraft flew past Pluto, which provided spectral data and imagery of the surface at resolutions as detailed as 80 m/pixel (*4*). The combination of Pluto's low gravity (0.62 m $s^{-1}$, or $1/12^{th}$ that of Earth), sparse atmosphere [1 Pa *(5)*], extreme cold [~ 45 K *(5)*] and surface composition [$N_2$, CO, $H_2O$ and $CH_4$ ices *(6)*] made pre-encounter predictions of surface processes challenging. However, pre-encounter speculation included that eolian processes, and potentially dunes, might be found on Pluto (*7*), because, despite the relatively thin atmosphere, the winds could possibly sustain saltation (i.e. particle movement by ballistic hops) in the current surface conditions. We examined images from the Long Range Reconnaissance Imager (LORRI) instrument (*8*) on New Horizons, taken during the probe's closest approach to Pluto, to search for landforms with the morphological and distributional characteristics of dunes. We also searched spectroscopic data from the Multispectral Visible Imaging Camera [MVIC *(9)*] for evidence of sufficient sand-sized ice particles to form dunes, and discuss how sublimation may play a role in lofting these particles enabling them to be saltated into dunes.

## Observations from New Horizons

The surface of Pluto, as revealed by New Horizons, is diverse in its range of landforms, composition and age (*4, 10*). One of the largest features, Sputnik Planitia (SP), is a plain of $N_2$, CO and $CH_4$ ice (*6* and Fig. S1) that extends across Pluto's tropics and at its widest point covers 30° of longitude (Fig. 1A). Polygonal features on the surface of SP, tens of kilometers across and bounded by trenches up to 100 m deep (Fig. 1B and 1C), have been interpreted as the result of thermally-driven, convective overturning of the ice (*11,12*), which, together with the uncratered surface of SP (4), suggests a geologically young (<500 ka; *11,12*) and active surface. Much of the western edge of the ice is bounded by the Al-Idrisi Montes (AIM), a mountainous region with relief of up to 5 km. On the SP plain bordering these mountains, distinct, regularly spaced, linear ridges are evident within a belt of approximately 75 km from the mountain margin (Fig 2A). They have positive relief as evident from shadows consistent with the mountains. The ridges show pronounced spatial regularity (~0.4 - 1 km wavelength), substantial length/width ratios (sometimes >20 km length), consistent shape along these lengths, and the presence of merging/bifurcation junctions (Fig. 1C and 1D; Fig. 2D and 2E). These junctions are approximately evenly spread between 47 north-facing bifurcations and 42 south-facing splits, and there is no clear spatial patterning to the direction of junctions. Farther from the mountain margin, toward the southeast, the ridges become more widely spaced and generally larger, while still in isolated fields or patches. Dark streaks are also found across the surface of the ice, typically behind topographic obstacles, and have been interpreted as wind streaks (*4*). These features indicate there are loose particles near and on the surface, as the streaks are thought to result from the deposition of suspended, fine particles in the lee of obstacles to wind flow (*4*, *5*, *13*; Fig. 1C, 1E).

We have identified 357 pale-colored, linear ridges on SP adjacent to the AIM (Fig. 2A, 2B, 2C), as well as six darker wind streaks in addition to the seven previously identified (4). The ridges closest to the SP/AIM mountain front are oriented approximately parallel with it, and ridges farther to the southeast shift orientation clockwise by ~30° over a distance of ~75 km (Fig. 2A and 2B); the ridges farther from the SP/AIM margin are significantly *(Mann-Whitney U = -7.41; p < 0.0001)* more widely spaced (Fig. 2C). Beyond the ~75 km-wide belt in which the linear ridges are predominantly found, the morphology of the surface changes, with preferential alignment of the ridges gradually disappearing (Fig. S2), until the landscape is dominated by weakly- or un-aligned, but still regularly dispersed, pits likely caused by sublimation of the ice (*14*). Wind streaks adjacent to the SP/AIM border are perpendicular to the ridges and mimic the shift in orientation shown by the ridges (Fig. 3A, 3B). Streaks within the zone in which the ridges are found (i.e. < 75 km from the SP/AIM border) are geographically (i.e. clockwise from north) oriented 113 ± 4° (1 standard deviation,σ, with sample number,n=4), whilst more distant wind streaks are oriented significantly [(*heteroscedastic Student's t = 9.912; p < 0.001* (Fig. 3B)] differently at 153 ± 10° (1σ, n=9).

**Interpretation as dunes**

The ridges found on western SP have morphological similarities to dunes (Figs. 1C, 1D, 4A, 4B and 4C). In addition to analogue similarities, we argue that these landforms are most consistent with an initial eolian depositional origin (i.e. dunes) on the grounds that: (a) a depositional origin is favored by the superimposition of many of the dunes on the trenches bordering SP's convective cells (Figs. 1D, 2D and 2E), (b) the distribution of the dunes with pattern coarsening (enlarging toward the southeast), away from the mountains (Fig. 4C), which is characteristic of dunefields; (c) their orientation, and systematic regional changes to this

orientation, are more readily explained by the wind regime than variations in incoming solar radiation; (d) the presence of pronounced wind streaks, orthogonal to the dunes, demonstrates the potential efficacy of Pluto's winds; (e) their location, on a methane- and nitrogen-dominated ice cap adjacent to mountains, is where the strongest winds and a supply of sediment might be expected, and; (f) their differing morphologies and undeformed regular alignment differs from the randomly aligned, shallow pits that border on the dune regions of SP (Fig. 4E and S2), and the deeply incised, discrete, aligned pits that can be found towards SP's southern and eastern margins (Fig. 4D). These pit-like features are morphologically distinct from the dune-like ridges farther north near the AIM that we discuss here (Figs. 4A and D). To test this hypothesis, we use a model (*15*) to examine the saltation of sand-sized (in this case, ~200-300 μm) particles on Pluto. Once initiated, the model indicates that saltation can be sustained even under the low (Earth-like; 1-10 m $s^{-1}$) wind speeds predicted at the surface today (*16*). However, the model also suggests that an additional process may be necessary to initially loft particles (*15*). This can be accomplished by sublimation, which is capable of lofting particles, and we model this process to find that particles can be entrained. This function of sublimation is in addition to the role sublimation may play in eroding mature dunes to more altered forms, which is also discussed in more detail below. Thus, under the current conditions, if there are sufficiently non-cohesive sand-sized particulates on the surface of Pluto, we should expect to find dunes.

Terrestrial and planetary dunes that form straight ridges can occur either perpendicular to the wind, forming transverse dunes, or parallel to the net local wind regime, forming longitudinal (or linear) dunes, and regional variation in the alignment of such dunes on earth is typically associated with meso or large scale atmospheric patterns (*17*). Wind streaks are well known on Venus and Mars, are present even under the tenuous atmosphere of Triton, and are generally

considered to represent the wind direction (*13*). The presence of pronounced wind streaks (Fig. 1C) within the dunefield, very nearly orthogonal to the dune trends, suggests that the observed dunes are transverse forms (Fig. 3A). The transverse nature of the dunes is further supported by the lack of consistency in bifurcation orientation; within dunefields oriented parallel to net sediment-transporting winds, such defects tend to cluster in terms of their orientation (*18*). The transverse orientation also shows that these ridges cannot be sastrugi (erosional snow ridges that form parallel to net winds) (*19*), or other erosional features analogous to yardangs (wind-carved ridges). The dunes in the northwestern portion of SP/AIM (Fig. 4A) are even more regularly spaced and parallel than many transverse dunes on Earth. Possible explanations for this include a highly consistent wind regime, lack of topographic deflection of winds, or a smooth substrate.

**Conditions for the formation of dunes and sublimation pits**

The existence of dunes on the surface of Pluto requires three necessary criteria to be met. Firstly, there must be a fluid atmosphere of sufficient density to make eolian transport possible. Secondly, there must be a granular material of a size and density, and with sufficiently low cohesion, that it can be entrained by winds. On Earth, this role is typically played by sand-sized mineral grains of a variety of compositions, including snow and ice. Thirdly, given the high wind speeds needed to lift surface particles against cohesion forces (*20*; Fig. 5), a specific mechanism must exist to loft large quantities of ice particles into the atmosphere where they are available for eolian transport. The presence of these criteria alone is necessary but not sufficient to identify the surface features as dunes. To justify our interpretation of these features as being dunes we also examine the conditions required for the other most likely candidate: aligned sublimation pits.

*Winds*

154 The orientations of the dunes and the wind streaks change locally, and consistently; in the case of
155 the dunes, over a distance on the order of 10-$10^2$ km. This implies that the topography and/or
156 surface composition has influenced the local wind regime, as was anticipated (*21*). These
157 orientations are consistent with sublimation-driven and topographic mechanisms for the
158 horizontal displacement of the atmosphere, as winds are generated by a gravity-driven flow
159 towards lower regions. Modeling of Pluto's current atmosphere suggests that surface winds on
160 the order of 1-10 $ms^{-1}$ are possible; they should be strongest where there are topographic
161 gradients and when driven by sublimation of surface ices by sunlight (*15*). The location of the
162 dunes at the western margins of the SP and AIM should thus be amongst the windiest locations
163 on the known regions of Pluto. As with Earth and Mars, once grain transport along the surface of
164 Pluto has begun, increased efficacy of grain-splash (the ejection of new particles due to grains in
165 saltation colliding with the ground) promotes a hysteretic effect that further sustains sediment
166 flux (*22, 23*). We use a numerical model (*15*) to demonstrate that despite the high wind speeds
167 needed for initial eolian entrainment, eolian transport can, once established, be sustained with
168 wind speeds of ~10 m $s^{-1}$ (Fig. 5).

169 *Sediment supply*

170 Although terrestrial dunes are typically associated with quartz, basalt or gypsum sand, other
171 materials can form the grains for dune development. Snow dunes of a very large scale are
172 observed in the center of the Antarctic continent (*24*); on Titan, it is generally assumed to be
173 atmosphere-derived organics, perhaps initially tholins, which form the equatorial belt of giant
174 dunes (*25*). While tholins are thought to form the dark patches of Pluto's equatorial regions (*6*),
175 the dunes evident on SP are light in color and are thus not formed from the same complex,
176 organic, photochemically-derived haze seen in Pluto's atmosphere (*4*). The most likely

candidates are thus $N_2$ and $CH_4$ ices. The surface of SP has generally been interpreted as predominantly composed of $N_2$ ice (*4, 5*), just as solidified nitrogen snows are believed to account for Triton's ice-covered surface (*26, 27*). The zone in which the ridges occur is coincident with the latitudes in which net $N_2$ condensation occurs over the course of a Pluto year (*16*; Fig. S3). However, recent analyses suggest that the composition may be a more complex mix of $N_2$, $CH_4$ and CO ices (*29*). Our analysis of data from the MVIC instrument, using a $CH_4$ filter (*15*) suggests that the location of the ridges and streaks coincides with a region of enhanced $CH_4$ ice content (Fig. S4). To the west of SP, the Enrique Montes in Cthulhu Macula (CM) have been shown to be capped with methane, presumably as the result of condensation or precipitation (*29, 30*). $CH_4$ ice retains hardness and rigidity under Pluto surface conditions, which is ideal for saltation and dune formation, while $N_2$ ice is likely to be softer. These constraints lead us to conclude that the dunes are formed predominantly of grains of methane ice, though we do not rule out that there could also be a nitrogen ice component. The presence of transverse forms, indicating sediment-rich local conditions, as opposed to more sediment-starved isolated barchans (discrete, crescentic dunes), suggests that locally, the sediment supply to this region of SP must be, or have been, abundant. Given the strength of the color and boundary delineations of methane in the AIM (Fig. S3), the methane ice may be quite thick and perhaps similar to valley glaciers in these isolated regions. If such high-altitude methane snowpack is a regular, seasonal occurrence, this may be a substantial reservoir from which to derive the abundant sand across the northwestern surface of SP required to form these transverse dunes.

*Grain size*

Credible sediment sizes are required for dune formation under the likely eolian regime. The grain sizes proposed for nitrogen ices (e.g., on Triton) have varied from micrometer (*31, 32*) to meter-

scale (*33*). We develop a method (*15*) to approximately constrain average grain size ($d$) and formative wind speed ($U$), from the mean crest-to-crest distance, or wavelength ($\lambda$), of the transverse dunes. For eolian dunes, the relevant length scale controlling this wavelength is the saturation length ($L_{sat}$) of the sediment flux, which is the distance needed by the flux to adapt to a change in local flow conditions. By combining theory (*34*), which predicts $L_{sat}$ as a function of wind speed and attributes of sediment and atmosphere, with a mathematical model (*35*) for $\lambda$ as a function of $L_{sat}$ and $U$, we obtain the values of $d$ and $U$ that are consistent with $\lambda$. These values are shown in Fig. S5, for $\lambda \approx 700$ m and $\lambda \approx 560$ m, which correspond to the transverse dunes far from and near to the mountainous area of Fig. 1, respectively. Given that expected formative wind speeds on Pluto are not larger than 10 m $s^{-1}$ (*16*), Fig S5 implies that grain size does not exceed ~370 μm and is most probably in the range between 210 and 310 μm. The spectral response of the MVIC $CH_4$ filter offers an additional constraint on the possible grain sizes observed, as Hapke modelling of the scattering within a granular medium provides a grain-size dependent control on the equivalent width of the absorption band. We find (*15*) that the observed response is consistent with a granular medium of ~200-300 μm.

*Lofting*

Although eolian transport can be maintained under Pluto's current wind regime, the speeds necessary for initial entrainment are orders of magnitude greater than those believed to be present at Pluto's surface (Fig. 5). An additional process is thus likely to be necessary to initiate eolian activity. In Sputnik Planitia, this process may be related to the intense, solar-driven sublimation of surface ices that injects more than $10^3$ $m^3$ $m^{-2}$ of gas in the atmosphere every afternoon (*16*, their figure 8). When sunlight penetrates through the upper layers of semi-transparent ice particles are lofted, sometimes at high vertical velocities, due to a mechanism

223 often referred to as a solid-state greenhouse (*36*). Therefore, initial entrainment of ice grains that
224 eventually form dunes may result from sublimating subsurface ice, as has been observed in the
225 thin atmospheres of Mars' northern polar region (*37*), and proposed for comet 67P/Churyamov-
226 Gerasimenko (*38*,*39*) and Triton (24,25). Modeling (*15*) suggests that subsurface $N_2$ sublimation
227 under Pluto surface conditions is capable of lofting even the densest candidate particles [$N_2$ ice, at
228 1030 kg $m^{-3}$, is denser than $CH_4$ ice, at 494 kg $m^{-3}$ (*40*)] with sizes ~200 μm, even at 0.1 Pa;
229 within the range of both Pluto's atmospheric pressure and the solid $N_2$ vapor pressure. Surface
230 ices of mixed composition offer an additional potential mechanism for facilitating grain lofting.
231 At the nitrogen frost point temperature of 63 K (*11*), pure methane ice particles mixed with
232 nitrogen should not sublimate at all. As methane particles are slightly heated by the sun, they
233 should enable the sublimation of the nitrogen ice that they touch and thus be readily lofted into
234 the atmosphere. Similar processes have recently been suggested for the migration of tholin
235 deposits on the surface of Pluto (*41*). Past periods of higher atmospheric pressures, which have
236 been suggested (*42*), could facilitate initial entrainment due to increased efficacy of eolian
237 processes.

238 *Sublimation*

239 The landscape of SP contains evidence of sublimation-driven landforms (*4*, *7*, *14*), and this
240 process is important in shaping parts of Pluto's surface. We consider whether the landforms
241 described here are more consistent with origins attributable to eolian or sublimation processes.
242 Locally, sublimation pits are deeply incised and may align to form linear troughs up to 10s of km
243 long and up to ~1 km deep (*4*, *7*). Frequently, and especially towards the southern and eastern
244 margins of SP, any alignment is subsequently heavily deformed, presumably driven by glacial
245 flow and convective overturning. Analogue landforms on Earth are provided by sublimation-

246 driven textures of snow and ice surfaces: ablation hollows (suncups) and penitentes (*14*, *43*). On
247 Earth, ablation hollows on snow may become aligned to leave ridges (penitentes), which align
248 themselves to within ±30° of east-west (i.e. the annual mean net sun path (*44*). Although the
249 orientation of any penitentes on Pluto is likely to be more complex and seasonally dependent,
250 they are only likely to form wavelengths in excess of ~1000 m (*45*). It is possible that
251 sublimation has acted upon already formed dunes in some regions (Fig. 2A). In polar regions on
252 Earth, wind-driven snow or ice grains can produce dunes, which then become hardened by
253 sintering and begin to undergo modification by wind and sublimation processes, thus changing
254 from depositional to erosional landforms (*44*, *45*). Given the tendency of ices to sinter together
255 under the right conditions, this could also happen in the $CH_4$ or $N_2$ ices of Pluto's dunes.
256 Sublimation erosion of Pluto's dunes may enlarge and round the areas between the dunes, and
257 sharpen the dune crests while preserving the overall dune orientation and spacing. This
258 morphology may be seen just at the resolution limit in the features farthest from the mountains in
259 Fig. 2a (enlarged view in Fig. S2). This is supported by modeling (*15*) of the net accumulation of
260 ices across Pluto's surface during the past two (Earth) centuries (Fig. S4), which suggests that for
261 the past ~30 Earth years, the dunefield has been experiencing net sublimation. Some of these
262 features may have progressed so far towards being erosional that we have not identified them as
263 dunes (Fig. S2).

264 *Age*

265 An upper limit on the age of the dunes, which sit atop the ice of the western margins of SP, is
266 imposed by the recycling rate of the upper surface of the convectional cells within the ice (i.e. <
267 500 ka) (*11*, *12*). This overturning of the substrate, inferred from the complete absence of
268 identified craters on SP, provides an age constraint for superficial landforms which is not

available for dunes on other solar system bodies, and implies a geologically and/or geomorphologically active surface (*4, 10, 46*). Surface features, undistorted by the convectional overturning within the ice, must be much younger than the timescales of convection, therefore closer to the timescales of Pluto's strong seasons (i.e. terrestrial decades – centuries). Further evidence that the dunes form on a timescale substantially shorter than that of the convection is suggested by the superposition of the dunes over the depressions at the cell margins (Fig. 1G).

## Summary and Conclusions

We have presented evidence that the highlands adjacent to SP accumulate methane. The ridged, dune-like landforms nearby, and accompanying wind streaks, are rich in methane relative to their underlying substrate. Although the wind speeds needed for eolian entrainment are higher than the likely wind speeds present on the surface, sublimation provides a credible mechanism for lofting grains. Numerical sediment transport and spectral modeling suggest these methane grains are approximately 200-300 μm. Our models suggest eolian transport is highly effective under Pluto surface conditions once initiated. An ample sediment supply appears to be available from a seasonally abundant snowpack in the adjacent mountains. The result is the formation of transverse dunes, as we identify in the images from New Horizons. The orientation of the dunes perpendicular to the wind is supported by the local topography and surface, and accompanying wind streaks. The presence of these dunes indicates an active atmosphere that produces geologically young landforms.

290 **References:**

291

292 1. Lorenz RD, Lunine JI, Grier JA, Fisher MA. Prediction of aeolian features on planets: Application to Titan
293 paleoclimatology. Journal of Geophysical Research-Planets. 1995;100(E12):26377-86.
294 2. Lorenz RD, Wall S, Radebaugh J, Boubin G, Reffet E, Janssen M, et al. The sand seas of Titan: Cassini
295 RADAR observations of longitudinal dunes. Science. 2006;312(5774):724-7.
296 3. Thomas N, Sierks H, Barbieri C, Lamy PL, Rodrigo R, Rickman H, et al. The morphological diversity of
297 comet 67P/Churyumov-Gerasimenko. Science. 2015;347(6220).
298 4. Stern SA, Bagenal F, Ennico K, Gladstone GR, Grundy WM, McKinnon WB, et al. The Pluto system:
299 Initial results from its exploration by New Horizons. Science. 2015;350(6258), aad1815.
300 5. Gladstone GR, Stern SA, Ennico K, Olkin CB, Weaver HA, Young LA, et al. The atmosphere of Pluto as
301 observed by New Horizons. Science (New York, NY). 2016;351(6279):aad8866.
302 6. Grundy WM, Binzel RP, Buratti BJ, Cook JC, Cruikshank DP, Ore CMD, et al. Surface compositions
303 across Pluto and Charon. Science. 2016;351(6279): aad9189.
304 7. Moore JM, Howard AD, Schenk PM, McKinnon WB, Pappalardo RT, Ewing RC, et al. Geology before
305 Pluto: Pre-encounter considerations. Icarus. 2015;246:65-81.
306 8. Cheng AF, Weaver HA, Conard SJ, Morgan MF, Barnouin-Jha O, Boldt JD, et al. Long-Range
307 Reconnaissance Imager on New Horizons. Space Science Reviews. 2008; 140(1):189-215
308 9. Reuter DC, Stern AS, Scherrer J, Jennings DE, Baer JW, Hanley J, et al. Ralph: A Visible/Infrared Imager
309 for the New Horizons Pluto/Kuiper Belt Mission. Space Science Reviews. 2008; 140(1):129-15410. Moore
310 JM, McKinnon WB, Spencer JR, Howard AD, Schenk PM, Beyer RA, et al. The geology of Pluto and Charon
311 through the eyes of New Horizons. Science. 2016;351(6279):1284-93.
312 11. McKinnon WB, Nimmo F, Wong T, Schenk PM, White OL, Roberts JH, et al. Convection in a volatile
313 nitrogen-ice-rich layer drives Pluto's geological vigour. Nature. 2016;534(7605):82-+.
314 12. Trowbridge AJ, Melosh HJ, Steckloff JK, Freed AM. Vigorous convection as the explanation for Pluto's
315 polygonal terrain. Nature. 2016;534(7605):79-+.
316 13. Sagan, C., Chyba, C. Triton's streaks as windblown dust. Nature. 1990; 346: 546 – 548.

14. Moore JM, Howard AD, Umurhan OM, White OL, Schenk PM, Beyer RA, et al. Sublimation as a landform-shaping process on Pluto. Icarus. 2017; 287: 320-333

15. Materials and methods are available as supplementary materials on Science Online.

16. Forget F, Bertrand T, Vangvichith M, Leconte J, Millour E, Lellouch E. A post-new horizons global climate model of Pluto including the N2, CH4 and CO cycles. Icarus. 2017; 287: 54-71.

17. Bagnold RA. The physics of blown sand and desert dunes. London: Chapman and Hall; 1941. 265 p 16.

18. Telfer MW, Hesse PP, Perez-Fernandez M, Bailey RM, Bajkan S, Lancaster N. Morphodynamics, boundary conditions and pattern evolution within a vegetated linear dunefield. Geomorphology. 2017; 290: 85-100

19. Warren SG, Brandt RE, Hinton PO. Effect of surface roughness on bidirectional reflectance of Antarctic snow. Journal of Geophysical Research-Planets. 1998;103(E11):25789-807.

20. Greeley R., Iversen JD. Wind as a Geological Process: on Earth, Mars, Venus and Titan. 1985; Cambridge University Press: Vol. 4. 67–106 .

21. Toigo AD, French RG, Gierasch PJ, Guzewich SD, Zhu X, Richardson MI. General circulation models of the dynamics of Pluto's volatile transport on the eve of the New Horizons encounter. Icarus. 2015;254:306-323.

22. Kok JF. An improved parameterization of wind-blown sand flux on Mars that includes the effect of hysteresis. Geophysical Research Letters. 2010;37.

23. Kok JF. Difference in the Wind Speeds Required for Initiation versus Continuation of Sand Transport on Mars: Implications for Dunes and Dust Storms. Physical Review Letters. 2010;104(7).

24. Frezzotti M, Gandolfi S, Urbini S. Snow megadunes in Antarctica: Sedimentary structure and genesis. Journal of Geophysical Research-Atmospheres. 2002;107(D18).

25. Soderblom LA, Kirk RL, Lunine JI, Anderson JA, Baines KH, Barnes JW, et al. Correlations between Cassini VIMS spectra and RADAR SAR images: Implications for Titan's surface composition and the character of the Huygens probe landing site. Planetary and Space Science. 2007;55(13):2025-36.

26. Hansen CJ, McEwen AS, Ingersoll AP, Terrile RJ. Surface and airborne evidence for plumes and winds on Triton. Science. 1990;250(4979):421-4.

27. Soderblom, LA, Kieffer SW, Becker TL, Brown RH, Cook AF, Hansen, CJ et al. Triton's geyser-like plumes – discovery and basic characterization. Science. 1990; 250 (4979); 410-415

344 28. Bertrand T, Forget F. Observed glacier and volatile distribution on Pluto from atmosphere-topography
345 processes. Nature. 2016; 540:86-89.
346 29. Schmitt B, Philippe S, Grundy WM, Reuter DC, Côte R, Quirico E et al. Physical state and distribution of
347 materials at the surface of Pluto from New Horizons LEISA imaging spectrometer. 2017. Icarus; 289:229-260.
348 30. Howard AD, Moore JM, Umurhan OM, White OL, Anderson RS, McKinnon WB, et al. Present and past
349 glaciation on Pluto. Icarus. 2017; 287:287-300.
350 31. Eluszkiewicz J. On the microphysical state of the surface of Triton. Journal of Geophysical Research-
351 Planets. 1991;96:19217-29.
352 32. Eluszkiewicz J, Stevenson DJ. Rheology of solid methane and nitrogen - applications to Triton.
353 Geophysical Research Letters. 1990;17(10):1753-6.
354 33. Zent AP, McKay CP, Pollack JB, Cruikshank DP. Grain metamorphism in polar nitrogen ice on Triton.
355 Geophysical Research Letters. 1989;16(8):965-8.
356 34. Pähtz T, Kok JF, Parteli EJR, Herrmann HJ. Flux Saturation Length of Sediment Transport. Physical
357 Review Letters. 2013;111(21): 218002.
358 35. Fourriere A, Claudin P, Andreotti B. Bedforms in a turbulent stream: formation of ripples by primary linear
359 instability and of dunes by nonlinear pattern coarsening. Journal of Fluid Mechanics. 2010;649:287-328.
360 36. Kaufmann E, Kömle NI, Kargl, G. Laboratory simulation experiments on the solid-state greenhouse effect
361 in planetary ices. Icarus, 2006;185:274-286
362 37. Thomas N, Hansen CJ, Portyankina G, Russell PS. HiRISE observations of gas sublimation-driven activity
363 in Mars' southern polar regions: II. Surficial deposits and their origins. Icarus. 2010;205(1):296-310.
364 38. Thomas N, Davidsson B, El-Maarry MR, Fornasier S, Giacomini L, Gracia-Berna AG, et al. Redistribution
365 of particles across the nucleus of comet 67P/Churyumov-Gerasimenko. Astronomy & Astrophysics. 2015;583:18.
366 39. Jia P, Andreotti B, Claudin P. Giant ripples on comet 67P/Churyumov–Gerasimenko sculpted by sunset
367 thermal wind. Proceedings of the National Academy of Sciences. 2017; 114(10): 2509–2514.
368 40. Fray N, Schmitt, B. Sublimation of ices of astrophysical interest: A bibliographic review.
369 Planetary and Space Science. 2009; 57: 2053-2080
370 41. Cruikshank D, paper presented 49th Division of Planetary Sciences meeting, Provo, UT, 15 October 2017.
371 Abstract ID 102.06.

372 42. Stern SA, Binzel RP, Earle AM, Singer KN, Young LA, Weaver HA, et al. Past epochs of significantly
373 higher pressure atmospheres on Pluto. Icarus. 2017; 287: 47-53.
374 43. Filhol S., Sturm M. Snow bedforms: A review, new data, and a formation model. Journal of Geophysical
375 Research – Earth Surface. 2015;120(9):1645-1669.
376 44. Cathles LM, Abbot DS, MacAyeal DR. Intra-surface radiative transfer limits the geographic extent of snow
377 penitents on horizontal snowfields. Journal of Glaciology. 2014;60(219):147-54.
378 45. Moores JE, Smith CL, Toigo AD, Guzewich SD. Penitentes as the origin of the bladed terrain of Tartarus
379 Dorsa on Pluto. Nature. 2017;541(7636):188-90.
380 46. Robbins SJ, Singer KN, Bray VJ, Schenk P, Lauer TR, Weaver HA et al. Craters of the Pluto-Charon
381 system. Icarus. 2017; 287: 187-206.
382 47. NASA/John Hopkins University Applied Physics Laboratory/South West Research Institute. The rich
383 colour variations of Pluto. Available at http://photojournal.jpl.nasa.gov/catalog/PIA19952 (accessed 27/09/2016)
384 48. NASA/John Hopkins University Applied Physics Laboratory/South West Research Institute. Pluto's Icy
385 Plains Captured in Highest-Resolution Views from New Horizons. Available at
386 http://photojournal.jpl.nasa.gov/catalog/PIA20336 (accessed 27/09/2016)
387 49. NASA/John Hopkins University Applied Physics Laboratory/South West Research Institute. Pluto's Close-
388 up, Now in Color. Available at: http://photojournal.jpl.nasa.gov/catalog/PIA20213 (accessed 27/09/2016)
389 50. NASA/John Hopkins University Applied Physics Laboratory/South West Research Institute. Ice Mountains
390 and Plains. Available at: http://photojournal.jpl.nasa.gov/catalog/PIA19954 (accessed 27/09/2016)
391 51. Sides SC, Becker TL, Becker KJ, Edmundson KL, Backer JW, Wilson TJ, et al., paper presented 48th
392 Lunar and Planetary Science Conference, held 20-24 March 2017, at The Woodlands, Texas. LPI Contribution No.
393 1964, id.2739
394 52. USGS Isis: Technical documents. Available at https://isis.astrogeology.usgs.gov/TechnicalInfo/index.html
395 (accessed: 27/03/2018).
396 53. Peterson J. New Horizons SOC to Instrument Pipeline ICD. 2007. Available at https://pds-
397 smallbodies.astro.umd.edu/holdings/nh-j-lorri-3-jupiter-v1.0/document/soc_inst_icd/ (accessed: 27/3/2018)
398 54. Kroy K, Sauermann G, Herrmann HJ. Minimal model for aeolian sand dunes. Physical Review E.
399 2002;66:031302.

400 55. Kok JF, Parteli EJR, Michaels TI, Karam DB. The physics of wind-blown sand and dust. Reports on
401 Progress in Physics. 2012;75(10).
402 56. Shao YP, Lu H. A simple expression for wind erosion threshold friction velocity. Journal of Geophysical
403 Research. 2000;105:22437-43.
404 57. Iversen JD, White BR. Saltation threshold on Earth, Mars and Venus. Sedimentology. 1982;29:111–9.
405 58. Almeida MP, Parteli EJR, Andrade Jr. JS, Herrmann HJ. Giant saltation on Mars. 2008;105:6222-6.
406 Proceedings of the National Academy of Science of the USA. 2008;105:6222-6.
407 59. Pähtz T, Kok JF, Herrmann HJ. The apparent surface roughness of a sand surface blown by wind from an
408 analytical model of saltation. New Journal of Physics. 2012;14:043035.
409 60. Sutton JL, Leovy CB, Tillman JE. Diurnal variations of the Martian surface layer meteorological
410 parameters during the first 45 sols at two Viking lander sites. Journal of Atmospheric Sciences. 1978;35:2346-2355.
411 61. Sullivan R, Greeley R, Kraft M, Wilson G, Golombek M, Herkenhoff K, et al. Results of the Imager for
412 Mars Pathfinder windsock experiment. Journal of Geophysical Research. 2000;105:24547–62.
413 62. Elbelrhiti H, Claudin P, Andreotti B. Field evidence for surface-wave-induced instability of sand dunes.
414 Nature. 2005;437:720-3.
415 63. Pye K, Tsoar H. Aeolian sand and sand dunes. London: Unwin Hyman; 1990. 396 p.
416 64. Matson DL, Brown RH. Solid-state greenhouse and their implications for icy satellites. Icarus. 1989:
417 77(1);67-81.
418 65. Piqueux S, Christensen PR. North and south subice gas flow and venting of the seasonal caps of Mars: A
419 major geomorphological agent. Journal of Geophysical Reseach – Planets. 2008:113;E06005.
420 66. Kaufmann E, Hagermann A. Experimental investigation of insolation-driven dust ejection from Mars' $CO_2$
421 ice caps. Icarus; 282:118-126
422 67. Hapke B. Theory of reflectance and emittance spectroscopy, Cambridge University Press, New York. 1993.
423 68. Grundy WM, Schmitt B, and Quirico E. The temperature-dependent spectrum of methane ice I between 0.7
424 and 5 micron sand opportunities for near-infrared remote thermometry. Icarus. 2002;155:486-496.
425 69. Bertrand T, Forget F, Umurhan OM, Grundy WM, Schmitt B, Protopapa S et al. The nitrogen cycles on
426 Pluto over seasonal and astronomical timescales. Icarus. 2018; 309:277-296.

**Acknowledgments:**

We thank all those involved, from concept to data retrieval, with the New Horizons mission. This research has made use of the USGS Integrated Software for Imagers and Spectrometers (ISIS).

**Funding:**

EP thanks the German Research Foundation for Grant RI2497/3-1. All New Horizons team member authors are funded by the NASA New Horizons Project.

**Author contributions:**

MWT conducted the spatial analysis and image interpretation, coordinated the research and co-wrote the paper. EJRP developed and conducted the numerical modelling and co-wrote the paper. JR coordinated the research and co-wrote the paper. RAB produced and provided LORRI mosaicking. TB and FF provided data on surface/atmosphere exchanges. FN performed calculations on the effectiveness of sublimation modelling. WMG conducted the Hapke modelling. JMM, SAS and JS contributed to the manuscript. TRL produced and provided LORRI mosaicking. RPB and AME provided circulation model data. HAW, CBO, LAY and KE are project scientists and contributed to the mansucript. KR provided discussion of ideas.

**Competing interests:**

There are no competing interests to declare.

**Data and materials availability:**

The LORRI data are archived in the Planetary Data System (PDS) Small Bodies Node at https://pds-smallbodies.astro.umd.edu/holdings/nh-p-lorri-3-pluto-v2.0/. MVIC data are available via the PDS at https://pds-smallbodies.astro.umd.edu/holdings/nh-p-mvic-3-pluto-v2.0/

**Supplementary Materials**

www.sciencemag.org

The New Horizons Geology, Geophysics and Imaging Science Theme Team

Materials and Methods

Figs. S1, S2, S3, S4, S5

References (51-69)

*Fig. 1. New Horizons fly-by imagery of landforms attributed to eolian origins. All images are unrectified and thus all scales are approximate. Color-composite MVIC images are shown here for context; dune identification was performed on greyscale LORRI images (shown below). A) Overview of Pluto centered on ~25° latitude, ~165° longitude, showing the locations of images B) and E) and figures 3A and S3 (47). B) The spatial context for SP and the AIM mountains to the west (48). Insets C) and D) show details of the highly regular spatial patterning which we attribute to eolian dune formation, and two newly-identified wind streaks (arrows x), along the margins of the SP/AIM border. Here the dunes show characteristic bifurcations (arrows y) and a superposition with SP's polygonal patterning (arrow z), suggesting a youthful age for these features (49). E) Two further wind streaks on the surface (x'), downwind of the Coleta de Dados Colles (4). These wind streaks, farther from the SP/AIM margin, are oriented differently to those close to the icefield's edge, and are still roughly orthogonal to the dunes there.*

*Fig. 2: Identified dunes (black lines) at the margins of western Sputnik Planitia (A). Prominent wind streaks are marked with orange lines. (B) Radial plot of the orientation of the dunes (n=331), and the direction orthogonal to the wind implied by the wind streaks close to the SP/AIM margin (orange dashed line; n=4; arithmetic mean, $\bar{x}$=203°). Because the dunes have a distinct shift in orientation (Fig. S1), the distribution of dunes in the three patches closest to the wind streaks within the dunefield (outlined in dashed green on A) has been separately highlighted on the radial plot, in green. These have a mean orientation of 204° (n=77), highlighted by the dashed green line. The dark blue line indicates the mean trend of the border of SP and the Al-Idrisi Montes in this area (194°). C) Frequency of dune spacings in clusters close to (red line representing dunes within the red dashed line of A) and far from (green line representing dunes within the green dashed line of A) the icefield/mountain interface. Dunes*

*farther from the mountains are significantly more widely-spaced ($\bar{x}$ = 700 m) than those close to the mountains ($\bar{x}$ = 560 m).D) Detail of the image interpretation process of the highest resolution swath, showing linear ridges, which sometimes bifurcate but are otherwise remarkable for their regularity; E) The same image with ridge lines highlighted*

*Fig. 3: The western margin of Sputnik Planitia. A) shows transverse dunes in black, the margin of the icefield and neighboring Al-Idrisi Montes to the northwest in blue, wind streaks close to this margin in orange, and further wind streaks further from the mountains in yellow. There is an orientation shift between the two sets of wind streaks, matching the correlation between the distance to the margin of the icefield and mountains, and the orientation of the transverse dunes (shown in inset B; wind streaks in orange). We interpret this as topography and/or surface composition influencing regional wind regimes.*

*Fig. 4: Analogues and comparison with sublimation features. A) details of the dunes on western Sputnik Planitia, centered on 34.35° 159.84° (location shown in Fig. 1). B) analogous terrestrial transverse dunes of the Taklamakan Desert, western China (image © CNRS/SPOT, © DigitalGlobe and courtesy of Google Earth™), and C) the same location down-sampled to a similar relative resolution as the Pluto dunes (i.e. approximately 5-10 pixels per crest-crest spacing). D) the aligned and distorted sublimation features abundant on southern and eastern SP (image centered on -4.78° 189.48°) and E) weakly-aligned to randomly oriented, shallow sublimation pits.. F) an example of a landscape revealing both eolian and sublimation-derived landforms at Mars' southern polar ice-cap from the Mars Reconnaissance Orbiter reveals both dark eolian bedforms (dunes and ripples), as well as sublimation pits developing in the underlying $CO_2$ ice (Image credit: NASA/JPL/University of Arizona, ESP_014342_0930_RED).*

500 *Fig. 5. Minimal threshold wind speed for initiation ($U_{ft}$, orange line) and continuation ($U_t$, black*
501 *line) of saltation on Pluto, at a reference height of 10 m above the soil, computed for different*
502 *values of the average particle diameter (15). The dashed horizontal line indicates maximum*
503 *likely windspeeds at Pluto's surface.*

504

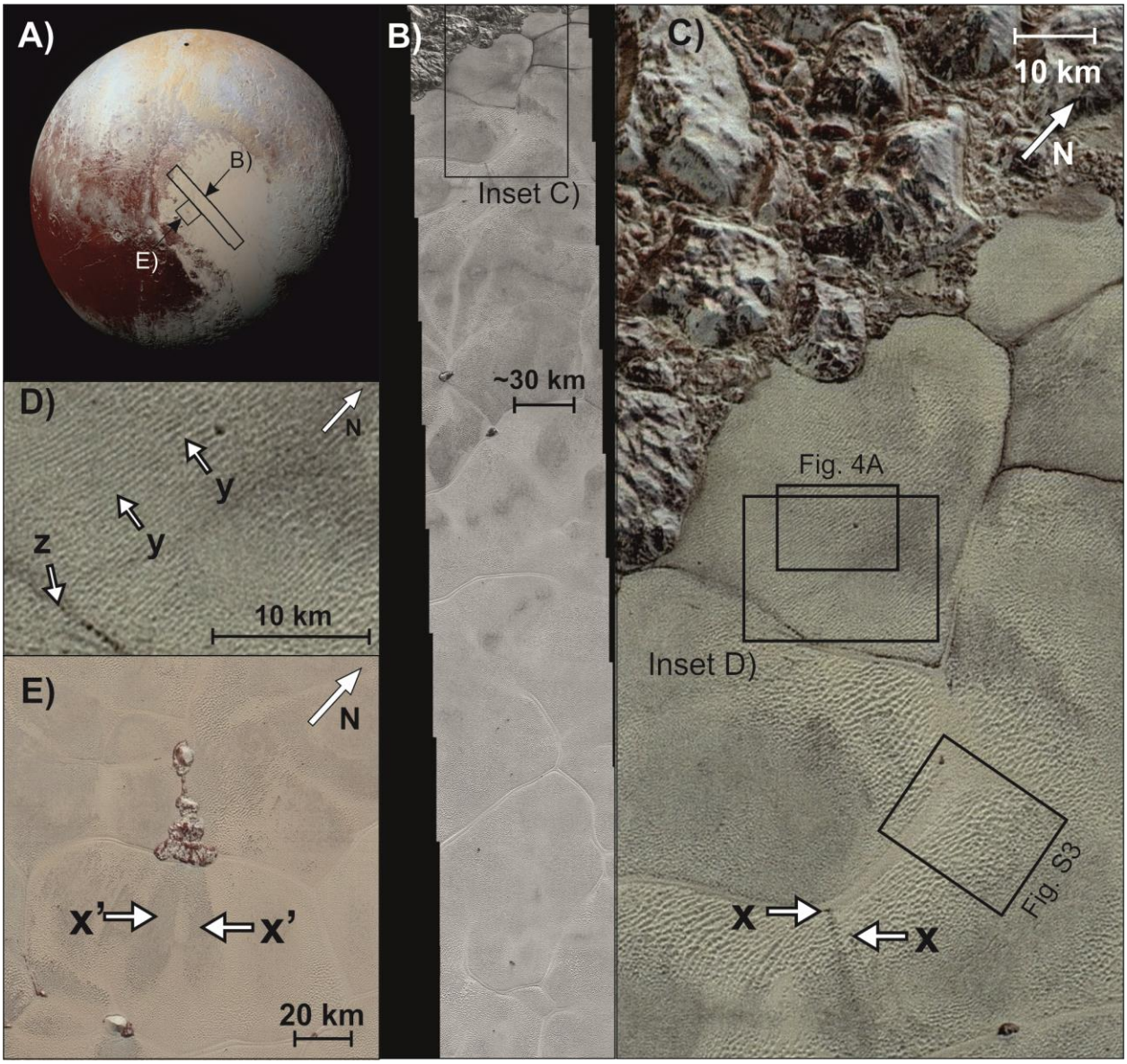
A)
B)
E)
B)
Inset C)
~30 km
C)
10 km
N
Fig. 4A
Inset D)
Fig. S3
D)
N
y
y
z
10 km
E)
N
x'
x'
20 km
x
x

*Fig. 1*

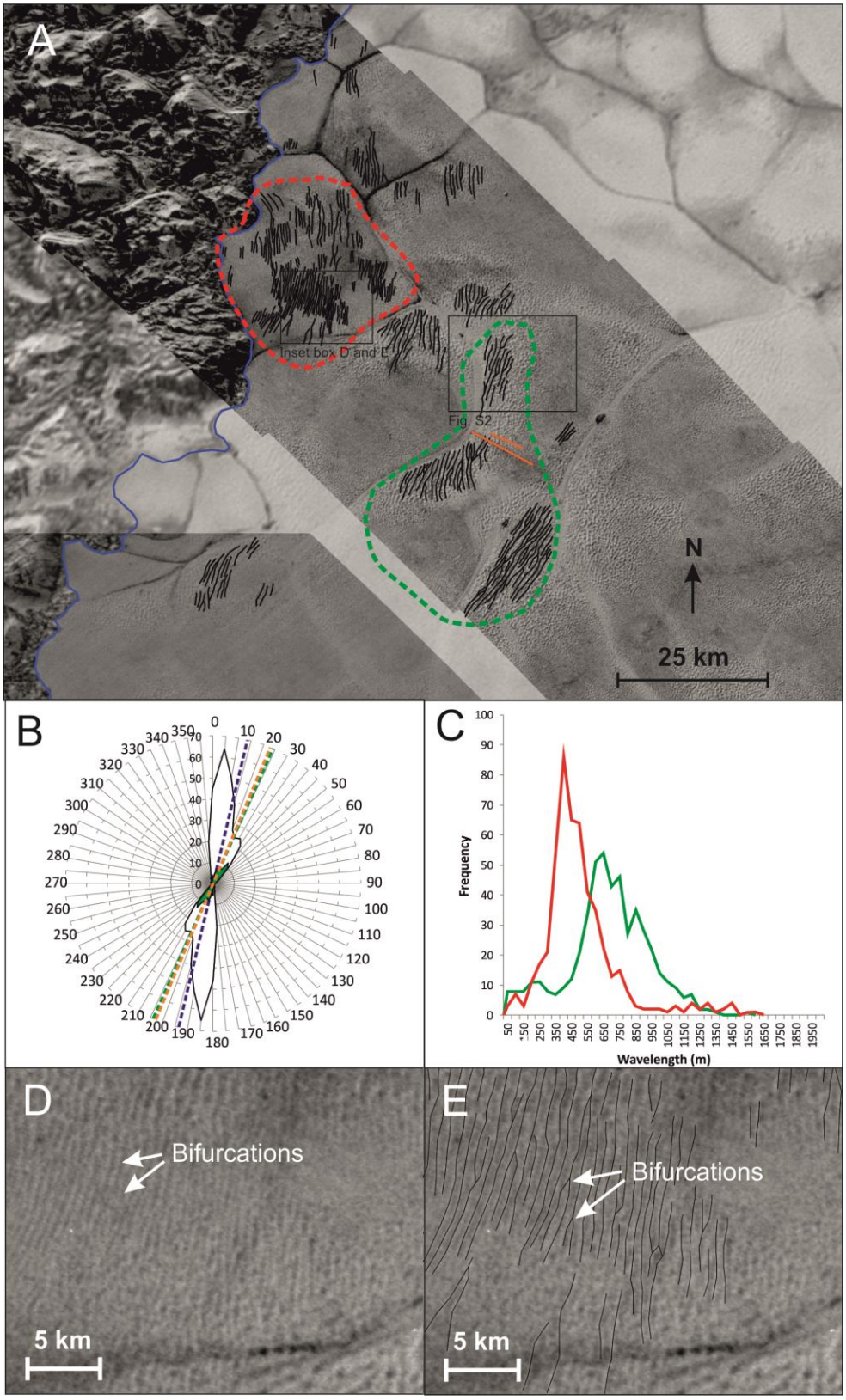
A
Inset box D and E
Fig. S2
N
25 km
B
C
Frequency
Wavelength (m)
D
Bifurcations
5 km
E
Bifurcations
5 km

*Fig. 2*

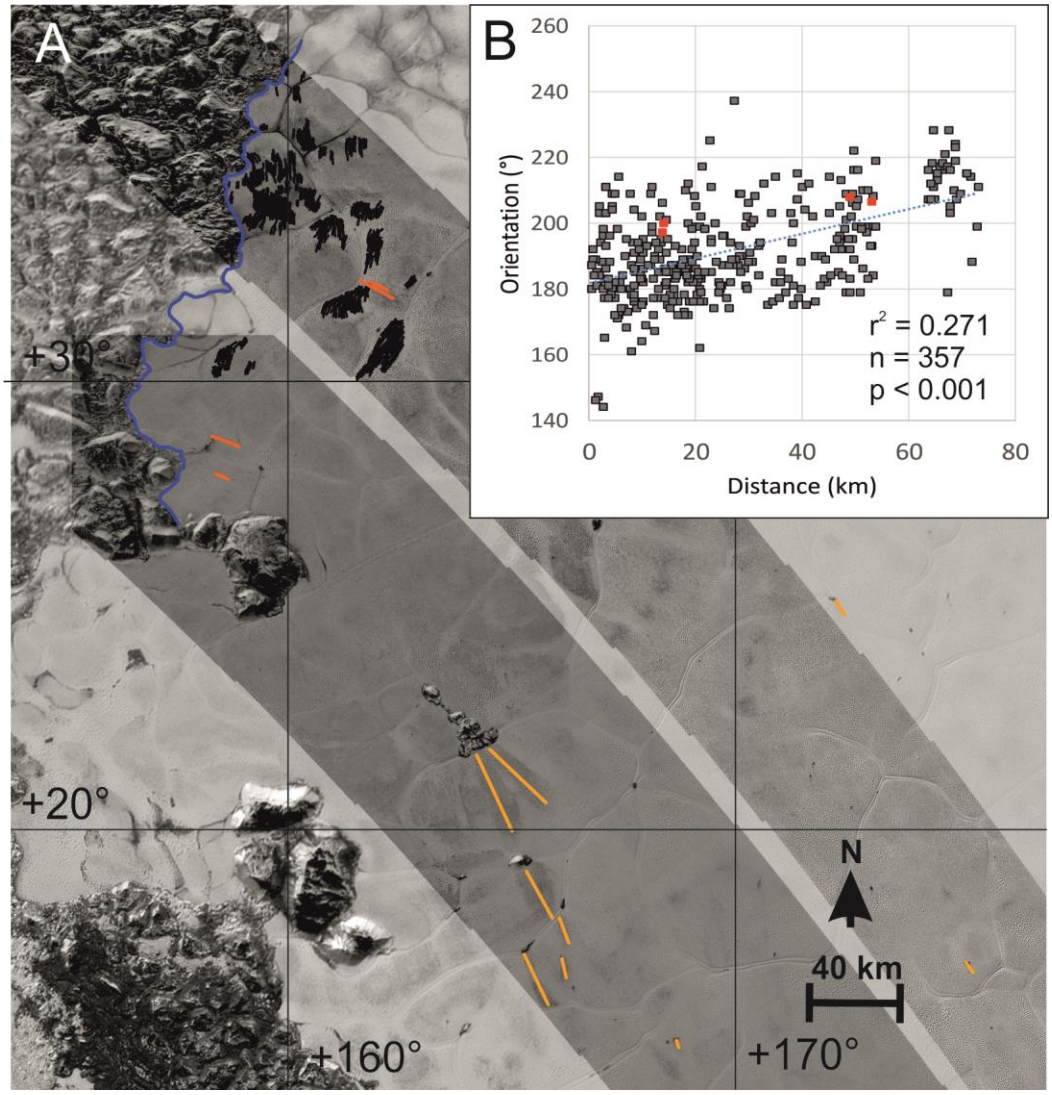
A
B
260
240
220
200
180
160
140
Orientation (°)
0
20
40
60
80
Distance (km)
r² = 0.271
n = 357
p < 0.001
+30°
+20°
+160°
+170°
N
40 km

Fig. 3

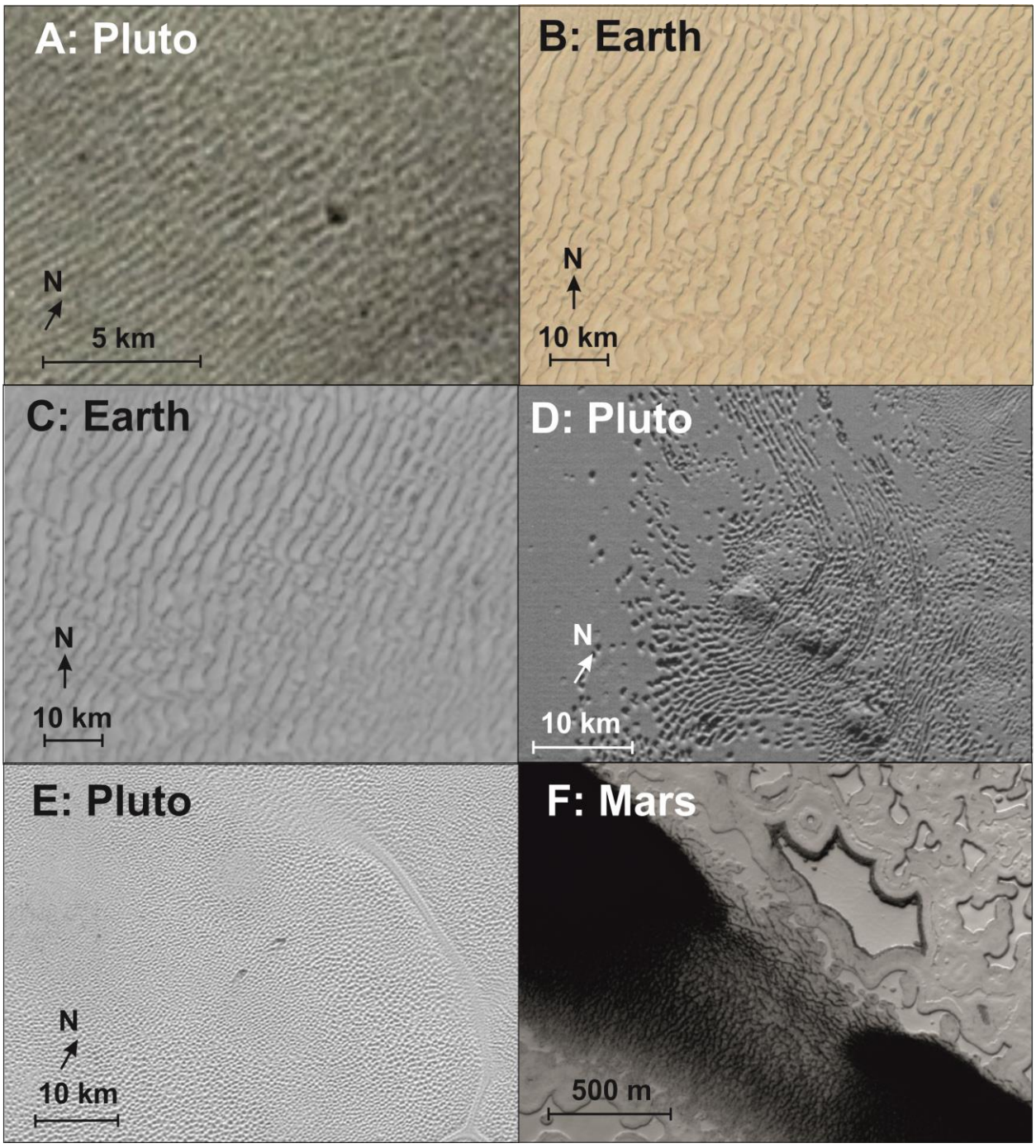
A: Pluto
N
5 km
B: Earth
N
10 km
C: Earth
N
10 km
D: Pluto
N
10 km
E: Pluto
N
10 km
F: Mars
500 m

*Fig. 4*

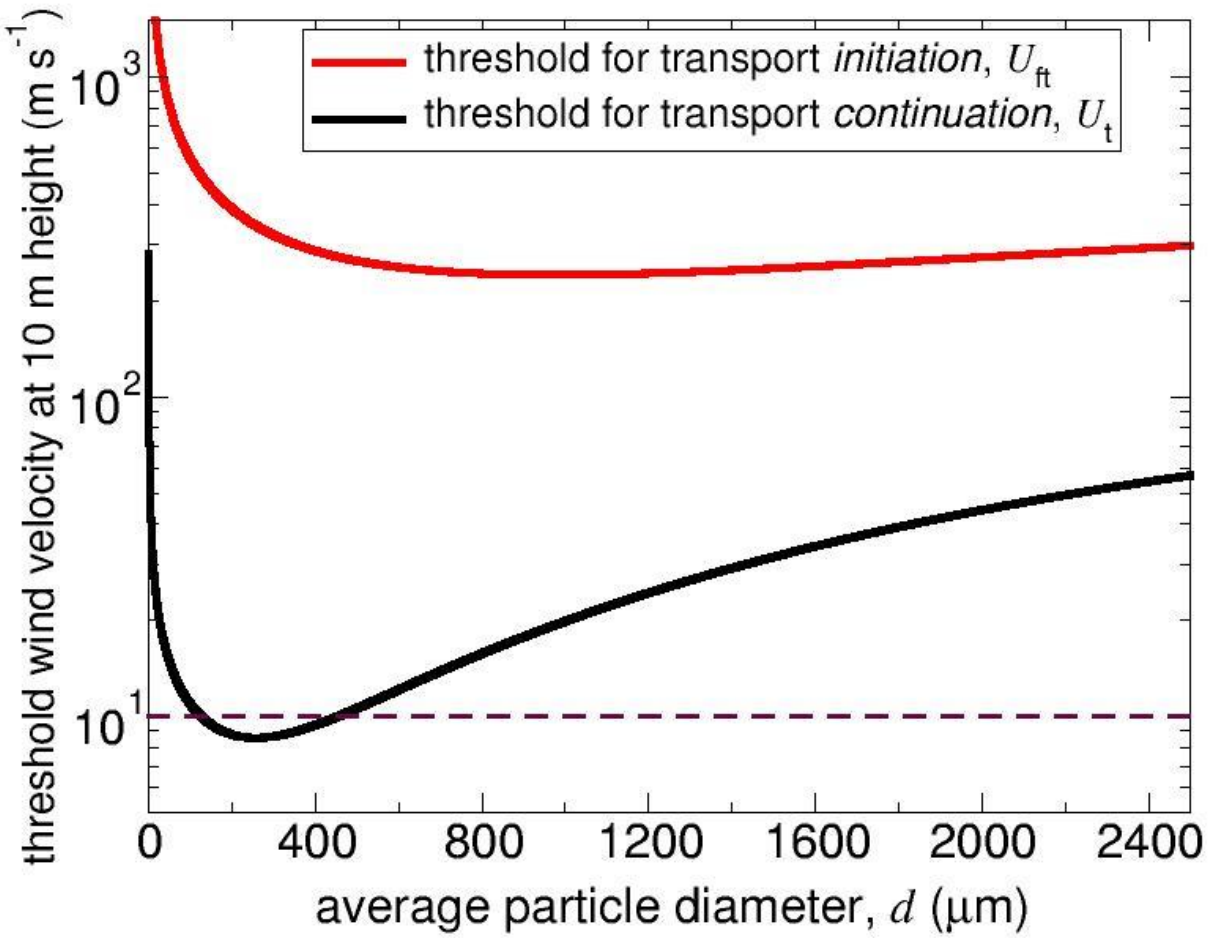
threshold for transport *initiation*, $U_{ft}$
threshold for transport *continuation*, $U_t$
threshold wind velocity at 10 m height (m s$^{-1}$)
$10^3$
$10^2$
$10^1$
0
400
800
1200
1600
2000
2400
average particle diameter, $d$ (μm)

*Fig. 5*

# Supplementary Materials for

## Dunes on Pluto

Matt W. Telfer, Eric J.R. Parteli, Jani Radebaugh, Ross A. Beyer, Tanguy Bertrand, François Forget, Francis Nimmo, Will M. Grundy, Jeffrey M. Moore, S. Alan Stern, John Spencer, Tod R. Lauer, Alissa M. Earle, Richard P. Binzel, Hal A. Weaver, Cathy B. Olkin, Leslie A. Young, Kimberley Ennico, Kirby Runyon, and the New Horizons Geology, Geophysics and Imaging Science Theme Team.

Correspondence to: matt.telfer@plymouth.ac.uk

**This PDF file includes:**

The New Horizons Geology, Geophysics and Imaging Science Theme Team Materials and Methods
Figs. S1 to S5

**The New Horizons Geology, Geophysics and Imaging Science Theme Team**

Jeffrey M. Moore, NASA Ames Research Center, Moffett Field, CA 94035.

Richard P. Binzel, Department of Earth, Atmosphere, and Planetary Science, Massachusetts Institute of Technology, Cambridge, MA 02139.

Marc W. Buie, Southwest Research Institute, Boulder, CO, USA.

Bonnie J. Buratti, Jet Propulsion Laboratory, California Inst. of Technology, Pasadena, CA.

Andrew F. Cheng, JHU/APL, Laurel, MD.

Kimberly Ennico, NASA Ames Research Center, Moffett Field, CA 94035.

W.M. Grundy, Lowell Observatory, Flagstaff, AZ.

J.J. Kavelaars, National Research Council of Canada, Victoria BC & Department of Physics and Astronomy, University of Victoria, Victoria, BC, Canada.

Ivan R. Linscott, Stanford University, Stanford, CA.

William B. McKinnon, Washington University in St. Louis, St. Louis, MO.

Catherine B. Olkin, JHU/APL, Laurel, MD

Harold J. Reitsema, Ball Aerospace (retired), Boulder, CO.

Dennis Reuter, NASA's Goddard Space Flight Center, Greenbelt, MD 20771.

Paul Schenk, LPI, Houston, TX.

Mark Showalter, SETI Institute, Mountain View, CA.

John Spencer  John R. Spencer, SwRI, Boulder, CO.

S. A. Stern, Southwest Research Institute, Boulder, CO, USA.

G. Leonard Tyler, Stanford (Emeritus), Stanford, CA.

H. A. Weaver, Johns Hopkins University Applied Physics Laboratory, Laurel, MD, USA.

565 Leslie A. Young, Southwest Research Institute, Boulder, CO, USA.

566

## Materials and Methods

### S 1 Image Interpretation

The names Sputnik Planitia and Al-Idrisi Montes are formally approved by the International Astronomical Union (IAU); all other names referred to within the text are informal.

Landforms were interpreted from the P_MVIC_LORRI_CA (75 m per pixel) and P_MPAN_LORRI (124 m per pixel) observations georeferenced to a global mosaic within ESRI ArcGIS 10.3, projected to a spheroid of radius 1188.3 km. The LORRI instrument is a panchromatic sensor in the range 350 to 850 nm with an unfiltered 1024 × 1024 pixel Charged-Couple Device (CCD). The field of view is 0.29° (*8*). A global LORRI image mosaic was used for contextualizing the area of interest. Images with variable resolutions (e.g. Fig. 1) are comprised of lower-resolution mosaics taken from more distant observations from the LORRI instrument, with superimposed swathes of higher spatial resolution images from the closest observations. For all LORRI image mosaics, the individual, PDS (Planetary Data System: https://pds.nasa.gov/) EDR (Experiment Data Record) images were processed using the Integrated Software for Imagers and Spectrometers (ISIS 3) (*51,52*). Images were converted from raw Data Numbers to *I/F* (the ratio of reflected to incident flux) units via radiometric equations (*53*). These images were then processed with the ISIS program *photomet* in order to correct for the range of illumination and viewing geometries, map-projected with the ISIS *cam2map* program, and finally mosaicked together with the ISIS *noseam* program.

Features were manually identified and digitized, based on an ontology limited to features with high length/width ratios (i.e. clear alignment) and a length of >1 km. Dune spacing was obtained by assigning 500 random points along the crest lines within dune ‘clusters’ using ArcGIS 10.3,

589 and using ArcGIS's Near function to find the distance to the nearest adjacent feature. Samples
590 near the end of isolated dunes thus might indicate a spuriously high spacing, which probably
591 accounts for the high outliers in Fig. 2.

592 MVIC consists of seven CCD arrays. Two are panchromatic, and four provide color or near
593 infrared detection capabilities (BLUE (400 to 550 nm filters), RED (540 to 700 nm), NIR (780 to
594 975 nm), and a narrow methane-sensitive band, based around the 890 nm absorption line
595 ("CH4," 860 to 910 nm). Fig. S4 is based on the highest resolution MVIC scan
596 ("P_COLOR_2"), with the unique MET ID 0299178092, archived in the PDS. Mid- observation
597 time was 2015-07-14 11:10:52 Coordinated Universal Time, corresponding to a range from
598 Pluto's center of 33963 km, sub-spacecraft longitude and latitude of 168.03 E, 25.98 N, and a
599 phase angle of 38.80°.
600

## S2 Modeling

This Section presents the equations used to obtain the minimal threshold wind velocities required for initiation and continuation of sediment transport, $U_{\mathrm{ft}}$ and $U_{\mathrm{t}}$, respectively (Fig. 5). Moreover, a description of the method developed for obtaining the average grain size $d$ and surface wind speed $U$ in the transverse dune field of Sputnik Planitia (Fig. S5) is provided.

In subsection **S2.1**, the equations for obtaining $U_{\mathrm{ft}}$ and $U_{\mathrm{t}}$ are shown, while in the three subsequent subsections, the method for obtaining $d$ and $U$ from the crest-to-crest distance of the transverse dunes is presented. As discussed in the main text, this distance scales with the saturation length of sediment transport, $L_{\mathrm{sat}}$, that is, the transient length needed by the mass flux of particles in the transport layer to adapt to a change in flow conditions (*34*). An analytical model for reliably computing $L_{\mathrm{sat}}$ as a function of the attributes of sediment and atmosphere in rarified atmospheres has been derived (*34*). In Subsection **S2.2**, we list the main equations of this model, which we use to compute $L_{\mathrm{sat}}$ in Sputnik Planitia as a function of grain size and wind speed. Moreover, an analytical model to obtain $L_{\mathrm{sat}}$ from the crest-to-crest distance of the "elementary" transverse dunes – which are the smallest transverse dunes formed by the wind on a flat sand surface – has been derived (*54*). In Subsection **S2.3** we list the equations of this model while in Subsection **S2.4** we present our method to constrain $d$ and $U$ in Sputnik Planitia by combining models (*34*) and (*35*).

Subsection **S2.5** considers these results in the light of the forces needed to loft a particle under surface and atmospheric conditions of SP. The final subsection, **S2.6**, justifies the assertion that the absorption of the MVIC $CH_4$ filter is consistent with the grain sizes proposed by the modelling of sections **S2.1** – **S2.4** are supported.

### S2.1 Threshold wind velocities for initiation and continuation of saltation on Pluto

#### *S2.1.1 Minimal threshold wind shear velocity for transport initiation, $u_{\mathrm{ft}}$*

Sediment transport begins when the wind shear velocity $u$, which is proportional to the mean flow velocity gradient in turbulent boundary layer flow, overcomes a minimal threshold value $u_{\mathrm{ft}}$. A mathematical model for $u_{\mathrm{ft}}$ is

obtained by balancing the entraining forces (aerodynamic lift and drag) against the stabilizing forces (attractive inter-particle forces and gravity), which leads to the following equation,

$$u_{\mathrm{ft}} \approx A_{\mathrm{N}} \sqrt{\frac{\rho_{\mathrm{p}} - \rho_{\mathrm{a}}}{\rho_{\mathrm{a}}} g d + \frac{\zeta}{\rho_{\mathrm{a}} d}} \quad \text{(S1)}$$

where $\rho_{\mathrm{p}}$ and $\rho_{\mathrm{a}}$ denote the densities of particles and air, respectively, $g$ is gravity, $d$ is the average diameter of the particles, $A_N \approx 0.1$ and $\zeta \approx 5 \times 10^{-4}$ N/m is an empirically determined parameter that scales with the strength of the attractive forces between the particles (*54, 55*). The first term in the square-root of Eq. S1 accounts for the balance between gravity and aerodynamic forces, while the second term incorporates the effect of attractive inter-particle forces (mainly van der Waals forces), which become significant when particle sizes decrease down to values below 60 $\mu$m. A different mathematical formulation for $u_{\mathrm{ft}}$, which leads to results not much different from the ones from Eq. S1, has been obtained (*56*). In this model, $A_{\mathrm{N}}$ is determined by empirical expressions that encode the effect of inter-particle cohesion; that is $A_{\mathrm{N}}$ depends on $d$, while $\zeta = 0$ (*56*).

*S2.1.2 Minimal threshold wind shear velocity for saltation continuation, $u_{\mathrm{t}}$*

Once initiated, eolian transport of the sediment particles along the surface can take place through several modes, in particular creep, that is, particles sliding or rolling along the surface, and saltation, which consists of particles moving through nearly ballistic loops, thereby ejecting new particles upon collision with the ground (splash). Moreover, once initiated, particle transport along the surface can be sustained at lower wind speeds because entrainment of new particles into flow occurs mainly as a consequence of grain-bed collisions. Under terrestrial conditions, the threshold for saltation continuation (or impact threshold) $u_{\mathrm{t}}$ is about 80% the threshold for saltation initiation, $u_{\mathrm{ft}}$ (*15*). However, recent theory and numerical simulations showed that the ratio $u_{\mathrm{t}}/u_{\mathrm{ft}}$ depends on atmospheric conditions. Specifically, this ratio may decrease substantially under conditions of lower atmospheric density and gravity, since such conditions lead to higher saltation trajectories, larger particle velocities and more intense splash (*57, 58*). This stronger hysteresis of the threshold wind speed for saltation in lower atmospheric density has been explicitly taken into account in theoretical work (*59*), which led to the following equation for $u_{\mathrm{t}}$,

$$u_t = \kappa(V_{rs} + V_0) \cdot [(1-\eta) \cdot \ln(z_{mt}/z_0)]^{-1}, \quad (S2)$$

where $\kappa = 0.4$ is the von Kármán constant; $V_{rs}$ is the steady-state value of the difference between particle and fluid velocities (*58*); $V_0$ is the average particle slip velocity – defined as the mean of the average horizontal (downwind) components of the particle velocities at ejection and impact, respectively; the constant $\eta = 0.9$ describes how efficiently the wind accelerates the grains within the transport layer at the threshold for sediment transport; $z_{mt}$ denotes an effective height of the average grain motion, and $z_0$ is the surface roughness of the quiescent bed.

The values of $V_{rs}$, $V_0$ and $z_{mt}$ are obtained from the following expressions (*58*),

$$V_{rs} = \sqrt{8\mu(s-1)gd/9 + (8\nu/d)^2} - 8\nu/d, \quad (S3)$$

$$V_0 = 16.2\sqrt{gd + 6\zeta/[\pi\rho_p d]}, \quad (S4)$$

$$z_{mt} = \beta\gamma\sqrt{V_{rs}V_t^3} \cdot [\mu g]^{-1}, \quad (S5)$$

where $s = (\rho_p - \rho_a)/\rho_a$, $\nu$ is the kinematic viscosity and $\mu$ stands for the Coulomb coefficient associated with the effective frictional force that the soil applies on the transport layer per unit soil area in the steady-state (*34*). For transport in the eolian regime, $\mu = 1$ (*34*). Furthermore, $\beta \approx 0.095$ is the ratio between the average work rate per unit soil area in the vertical motion and that in the horizontal motion and $\gamma = z_{mt}/z_s \approx 0.17$, with $z_s$ standing for the characteristic height of the exponential decay of the grain-borne shear stress, while $V_t$, the average grain velocity at threshold, is given by the equation,

$$V_t = V_0 + \eta V_{rs}/[1-\eta]. \quad (S6)$$

Moreover, the surface roughness $z_0$ is given by the equation (*55*),

$$z_0 = d\exp(-\kappa B), \quad \text{(S7)}$$

where

$$B = 8.5 + \left[2.5\ln(R_p) - 3\right]\cdot\exp\left\{-0.11\left[\ln(R_p)\right]^{2.5}\right\}, \quad \text{(S8)}$$

with $R_p = u_t d/\nu$.

*S2.1.3 Minimal threshold wind shear velocities under atmospheric conditions of Pluto*

We calculate the minimal threshold wind shear velocity $u_{ft}$ as a function of the particle diameter using Eq. S1, with Pluto's gravity $g = 0.658$ m/s$^2$, methane ice particles of density $\rho_p = 494$ kg/m$^3$ and an atmospheric density $\rho_p = 9.1 \times 10^{-5}$ kg/m$^3$, consistent with surface temperature of 37 K and pressure of 1 Pa atmosphere composed predominantly of $N_2$ (*5*).

Moreover, the minimal threshold wind shear velocity $u_t$ for sustained transport is computed as a function of average grain diameter under the attributes of atmosphere specified in the previous paragraph (the associated kinematic viscosity is $\nu$ = 0.02 m$^2$/s).

From $u_t$ and $u_{ft}$, the corresponding threshold wind speeds at the reference height of 10 m can be computed using the equation

$$U = \frac{u}{\kappa}\ln\frac{z}{z_0}, \quad \text{(S9)}$$

where $z$ is the height above the ground. By taking $z = 10$ m and $z_0$ computed with Eq. S7 as a function of the mean particle size $d$, and by substituting the values of $u_{\mathrm{ft}}$ and $u_{\mathrm{t}}$ obtained with Eqs. S1 and S2, respectively, as functions of $d$, we obtain the result shown in Fig. 5.

We see that grain sizes between 100 and 400 $\mu$m correspond to the lowest wind velocities required to sustain sediment transport. The associated wind shear velocities are between 0.4 and 0.6 m/s. These wind shear velocities are common to sand deserts of the Earth and fall within the range of average values of $u$ measured on Martian soils (60,*61*).

S2.2 Flux saturation length of eolian sediment transport on Pluto

The saturation length of the eolian sediment flux is computed using the equation (*34*)

$$L_{\mathrm{sat}} = 3c_v V_{\mathrm{s}} V_{\mathrm{rs}} F K \mu^{-1} g^{-1} \quad \text{(S10)}$$

where $c_v \approx 1.3$ is the steady-state value of the particle speed square correlation, obtained from measurements of the particle velocity distribution (*34*). The average particle velocity in the steady-state, $V_{\mathrm{s}}$, is given by the equation

$$V_{\mathrm{s}} = V_{\mathrm{t}} + [3u_{\mathrm{t}}/2\kappa] \cdot \ln(V_{\mathrm{s}}/V_{\mathrm{t}}) + [u/\kappa] \cdot F_{\gamma}(u_{\mathrm{t}}/u), \quad \text{(S11)}$$

where

$$F_{\gamma}(x) = (1-x) \cdot \ln(1.78\gamma) + 0.5(1-x^2) + E_1(\gamma) + 1.154(1 + x \ln x)(1-x)^{2.56} \quad \text{(S12)}$$

with $E_1(x)$ standing for the exponential integral function (*34, 58*). Moreover, the variables *F* and *K* are given by the expressions

$$F = [V_{rs} + 16\,\nu/d] \cdot [2V_{rs} + 16\,\nu/d]^{-1}, \quad \text{(S13)}$$

$$K = \frac{1 + F^{-1}[(V_s + V_{rs})/(2V_{rs})][(u/u_t)^2 - 1]}{1 + [(V_s + V_{rs})/(2V_s)][(u/u_t)^2 - 1]}. \quad \text{(S14)}$$

By obtaining the saturation length from the dune size, it is possible to constrain possible values of $u$ and $d$ formative of the transverse dunes. This procedure is explained in the next two subsections.

S2.3 Flux saturation length from the crest-to-crest distance of the elementary transverse dunes

The flux saturation length can be obtained from the wavelength (crest-to-crest-distance) of the smallest transverse dunes that a wind forms on a flat sand sheet ("elementary transverse dunes") using an analytical model (*35*). Examples of such elementary transverse dunes are superimposed bedforms emerging on a flat surface or on top of a large barchan dune, for instance due to a storm wind that makes a small angle with the prevailing transport direction (*62*). An important assumption we have to make to use this model is, thus, that the size of dunes observed in the images (~ 700 m) is not substantially larger than the size of the elementary dunes produced by the action of wind on a flat sand sheet on Pluto. That is, the dunes did not increase significantly in size due to amalgamation and merging into much larger or giant bedforms; to compare, the size of elementary dunes on Earth and Mars is about 10 m and 100 m, respectively (*55*). This is a plausible assumption for the dune field of Sputnik Planitia given the very young age of this field, as discussed in the main text. The spatial wind shear stress on top of a flat bed with small perturbation $h(x)$ in the vertical direction can be computed (*35*). The Fourier-transformed shear stress $\hat{\tau}(k)$ can be written as:

$$\hat{\tau} = \tau_0(A + iB)k\hat{h}, \quad \text{(S15)}$$

where ^ denotes the Fourier-transformed value of the corresponding quantity, $k$ is the wavenumber, and $A$ and $B$ can be approximated by the expressions (*34*),

$$A(R) = 2 + \frac{1.072 + 0.093069R + 0.10838R^2 + 0.024835R^3}{1 + 0.041603R^2 + 0.0010625R^4}, \quad \text{(S16)}$$

$$B(R) = \frac{0.036989 + 0.15765R + 0.11518R^2 + 0.0020249R^3}{1 + 0.0028725R^2 + 0.00053483R^4}, \quad \text{(S17)}$$

with $R = \ln(2\pi/\kappa z_0^*)$. The wavelength $\lambda = 2\pi/k_{\max}$ of the dunes corresponds to the wavenumber $k_{\max}$ under which the dunes grow fastest. By using instability analysis (*35*), it has been shown that $\lambda$ is related to the saturation length $L_{\text{sat}}$ through the equation,

$$\frac{2\pi L_{\text{sat}}}{\lambda} = X^{-1/3} - X^{1/3}, \quad \text{(S18)}$$

where the quantity $X$ is defined as,

$$X = -\frac{\tilde{B}}{\tilde{A}} + \sqrt{1 + \frac{\tilde{B}^2}{\tilde{A}^2}}, \quad \text{(S19)}$$

while $\tilde{A}$ and $\tilde{B}$ incorporate dependence on the flow shear velocity ($u$),

$$\tilde{A} = A(R_{\max}) - \frac{\gamma_c A(R_{\max})}{1 + \gamma_c} \cdot \frac{u_t^2}{u^2}, \quad \text{(S20)}$$

$$\tilde{B} = B(R_{\max}) - \frac{\gamma_c B(R_{\max}) + \mu_c^{-1}}{1 + \gamma_c} \cdot \frac{u_t^2}{u^2}. \quad \text{(S21)}$$

In the equations above, $R_{\max} = \ln[2\pi/(k_{\max} z_0^*)] = \ln[\lambda/z_0^*]$, $\mu_c \approx \tan(32°)$ is the dynamic angle of repose of the sand, and $\gamma_c \approx 0$ for eolian transport.

The apparent roughness $z_0^*$, which is the surface roughness in the presence of the transport layer, is obtained from the equation,

$$\ln\left(\frac{z_0^*}{z_0}\right) = \left(1-\frac{u_t}{u}\right)\ln\left(\frac{z_s}{1.78z_0}\right) - 1.154\left[1+\frac{u_t}{u}\ln\left(\frac{u_t}{u}\right)\right]\left(1-\frac{u_t}{u}\right)^{2.56}, \qquad \text{(S22)}$$

with $z_s = z_{mt}/\gamma$.

S2.4 Grain size and wind speed that formed the transverse dunes of Sputnik Planitia

Our method to obtain the possible values of $u$ and $d$ (or, equivalently, $U$ and $d$) that formed the transverse dunes in Sputnik Planitia consists of numerically solving the following equation,

$$L_{sat;d,u} = L_{sat;\lambda}, \quad \text{(S23)}$$

where $L_{sat;d,u}$ denotes the right-hand side of Eq. S10 and $L_{sat;\lambda}$ is obtained from Eq. S18, that is, $L_{sat;\lambda} = \left[X^{-1/3} - X^{\frac{1}{3}}\right]\cdot\lambda/(2\pi)$.

By solving Eq. S23, and using Eq. S9 to obtain the wind velocity at 10 m height, we obtain Fig. S5. This shows the only values of $d$ and $U$ that lead to transverse dunes with spacing $\lambda$ = 560 m and $\lambda$ = 700 m, which are the values observed at the transverse dune field of Sputnik Planitia (see main text). From Fig. S5 we see that the transverse dunes consist of grain sizes that are, on average, not larger than ~370 μm (for the larger average crest-to-crest distance of 700 m). Considering that the most probable wind speeds are within the region below this horizontal line in Fig. S5, it can be seen from this figure that the characteristic grain size of the transverse dunes is not smaller than ~210 μm. Furthermore, given the upper bound of 10 m/s, the grain size leading to the observed crest-to-crest distances is most probably within the range $210 \lesssim d\ /\mu m \lesssim 310$ (see Fig. 3B). This range of grain sizes corresponds to the following most probable range of wind velocity $U$ at 10 m height (see Fig. 3B): $8.5 \lesssim U/(\mathrm{m/s}) \lesssim 10$.

These ranges of grain size and wind velocity are fully consistent with the average size of sediments composing Earth dunes and wind speed formative of eolian bedforms in terrestrial dune fields (*17, 60*).

S2.5 The role of sublimation in initial particle lofting

Given the high shear velocities required for initial entrainment of particles under Pluto's surface conditions, here we explore the feasibility of sublimation as a mechanism for particle lofting. The complexities of considering the sublimation of the likely mixed-ice composition (probably $CH_4$ and $N_2$) of the surface of SP are substantial, and thus here we consider the most conservative scenario for lofting particles; that the sediment comprising the dunes is the denser $N_2$ ice.

Solid-state greenhouse effects have been shown to heat the subsurface (*64*), and the effects of this in generating ejecta have been demonstrated theoretically (*65*) and experimentally (*66*) in thin atmospheres. If a subsurface cavity is exposed to the surface by sublimation, the initial escape velocity will be the thermal velocity (~100 $ms^{-1}$). Resultant drag imposed on particles, per unit area, is approximated by $\rho v^2$ where ρ is the fluid density and $v$ the fluid velocity. Using the ideal gas law and considering the weight of the particle, we can thus state that:

$$v = \frac{\sqrt{r\rho_s gRT}}{P\mu} \qquad \text{(S24)}$$

where $r$ is the particle radius, $\rho_s$ is the particle density, $g$ is gravity, $R$ the gas constant, $T$ the gas temperature, $P$ the gas pressure and $\mu$ the molar mass of the gas. Using conservative Pluto surface conditions, and solving for $P$, the pressure needed to support a particle 200 μm in radius is only 0.1 Pa at 50K. However, this should be regarded as an indicative figure rather than a definitive answer, as a number of complications could change this value. These include the likely overestimate of the effective velocity due to atmospheric interaction, and the complications likely to result from rate of the sublimation of lofted particles. Conversely, the likely scenario of mixed-composition ices may favor particle lofting; at the nitrogen frost point temperature, pure methane ice particles mixed with nitrogen

should not sublime at all. As they are slightly heated by the sun, they should sublimate the nitrogen ice that they touch and be readily put aloft by the condensation flow, and thus provide an initial entrainment.

S2.6 Modeling the size of particles responsible for the MVIC $CH_4$ filter observation

New Horizons' Multi-Spectral Visible Imaging Camera (MVIC) has four interference filters, one of which passes wavelengths from 860 to 910 nm, where $CH_4$ ice has a characteristic absorption band (*9*). Using this filter, along with two others covering 540-700 nm and 780-975 nm, it is possible to estimate the equivalent width of absorption in the $CH_4$ filter, which can be attributed to $CH_4$ ice. This $CH_4$ equivalent width has been mapped on the encounter hemisphere (*6*). Examining the study area shows that many of the areas identified as having dunes or wind streaks show greater $CH_4$ absorption than surrounding areas, as shown in Fig. S4, where the equivalent width map is superposed in pink on New Horizons LORRI imagery of the region. The $CH_4$ equivalent width varies across the scene from around 0.5 nm at lower right to as high as 3 nm corresponding to the centers of some of the convection cells near Al-Idrisi Montes. Localized areas of much higher absorption can be seen within Al-Idrisi, and could represent potential sources of $CH_4$ ice particles.

To check if 200 to 300 micron $CH_4$ ice particles could produce the observed absorption, we ran Hapke models (e.g. *67*) to account for the multiple scattering effect in a granular medium. For this region, the incidence angle is about 41 degrees, emission angle is about 5 degrees, and phase angle is 39 degrees, so the observation was well outside of any opposition surge, and thus we set B_0 to zero. We used Hapke's equivalent slab model to compute the single scattering albedo as a function of wavelength, setting the real part of the refractive index to a constant 1.3 and the imaginary part to 40 K values (*68*). We assumed an isotropic single scattering phase function. For 200 micron particles, the model produced a spectrum in which the $CH_4$ equivalent width was 3.8 nm and for 300 micron particles, we found an equivalent width of 4.7 nm. These values are somewhat higher than what was observed in the MVIC images, but would be consistent with patchy coverage by $CH_4$ ice particles in that size range in the areas of northwest SP where $CH_4$ absorption was strongest.

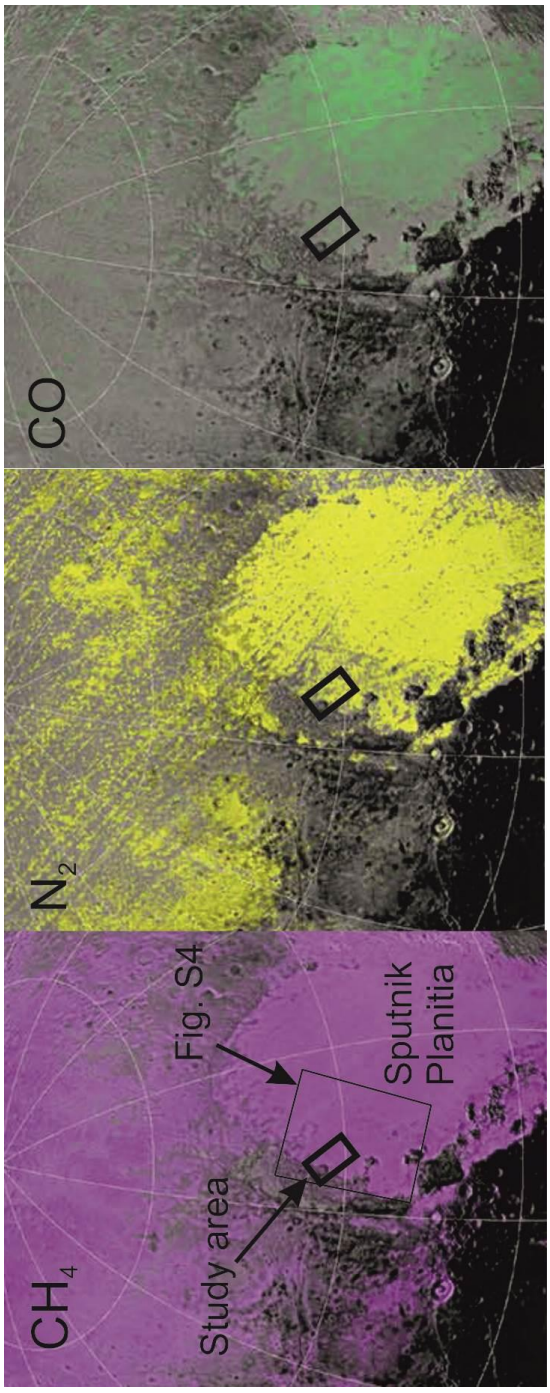


**Fig. S1.**

Position of the dunes (within the box) overlaid on the surface compositions (*6*) of A) methane, $CH_4$, B) nitrogen, $N_2$, and C) carbon monoxide, CO. The location of the dunefield at the western margin of Sputnik Planitia shows a surface composition dominated by $N_2$ and $CH_4$ ices. The location of Fig. S4 is also indicated here. Figure modified from (*6*).

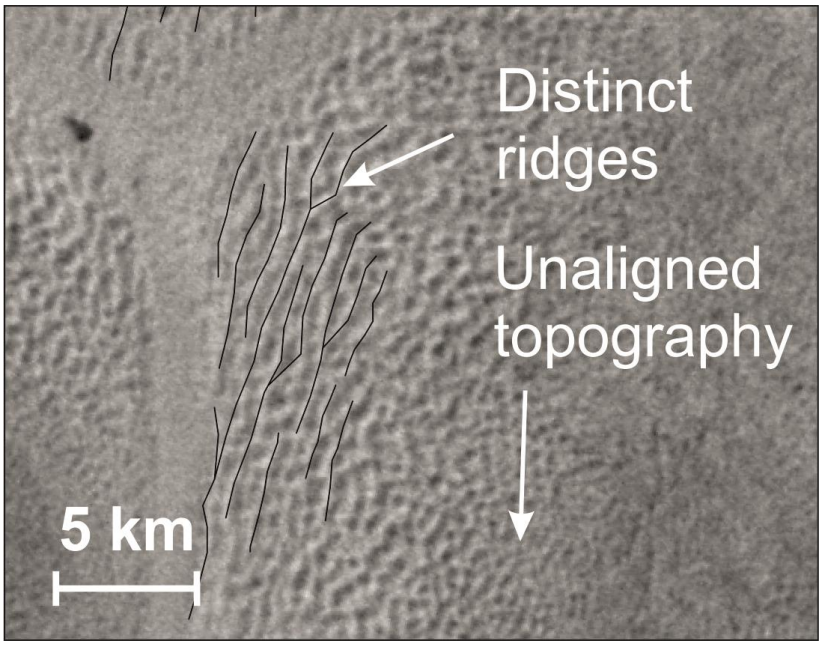


**Fig. S2**

Fig. S2. The edge of the area of distinct linear features, where the surface changes to an unaligned, scalloped relief. Location shown on Fig. 1.

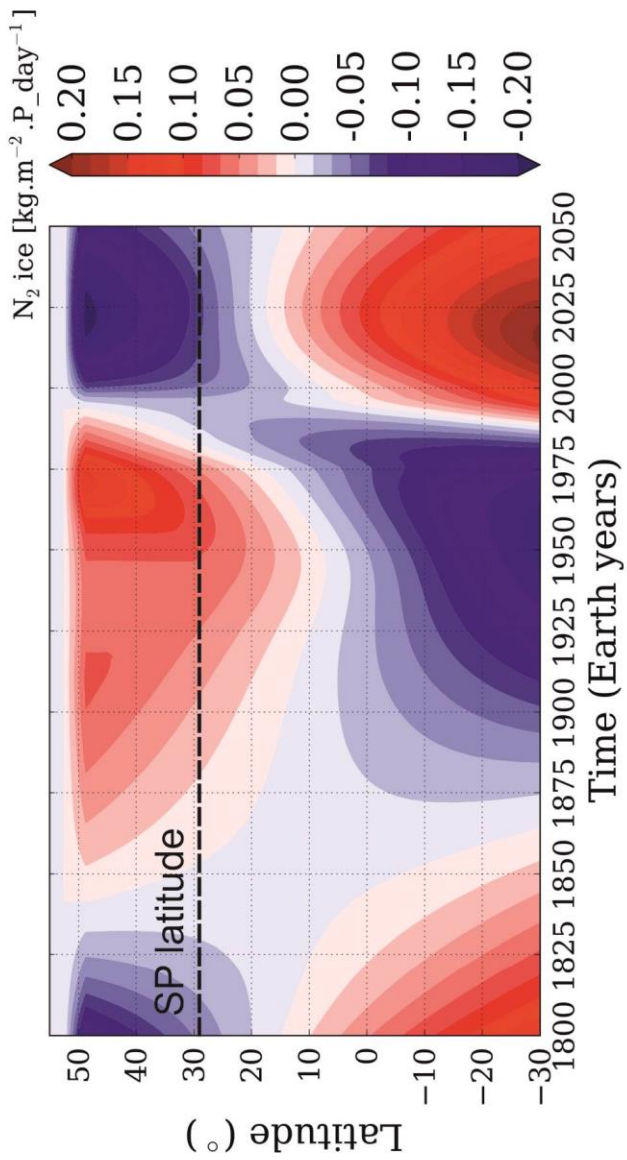


**Fig. S3**

The accumulation and loss of $N_2$ ice over a timescale covering approximately one Pluto year (here from the terrestrial period 1800 to 2015), obtained with a volatile transport model within a post-encounter Pluto General Circulation Model (the model described in *16* and *69*). Note that at +35°, $N_2$ ice condensed in SP from 1820 to 1955 with a rate of few tens of micrometers per day (P_day refers to one Pluto day), whereas currently it is experiencing net sublimation. This is consistent with the observed degradation of eolian landforms following a period of enhanced sediment supply.

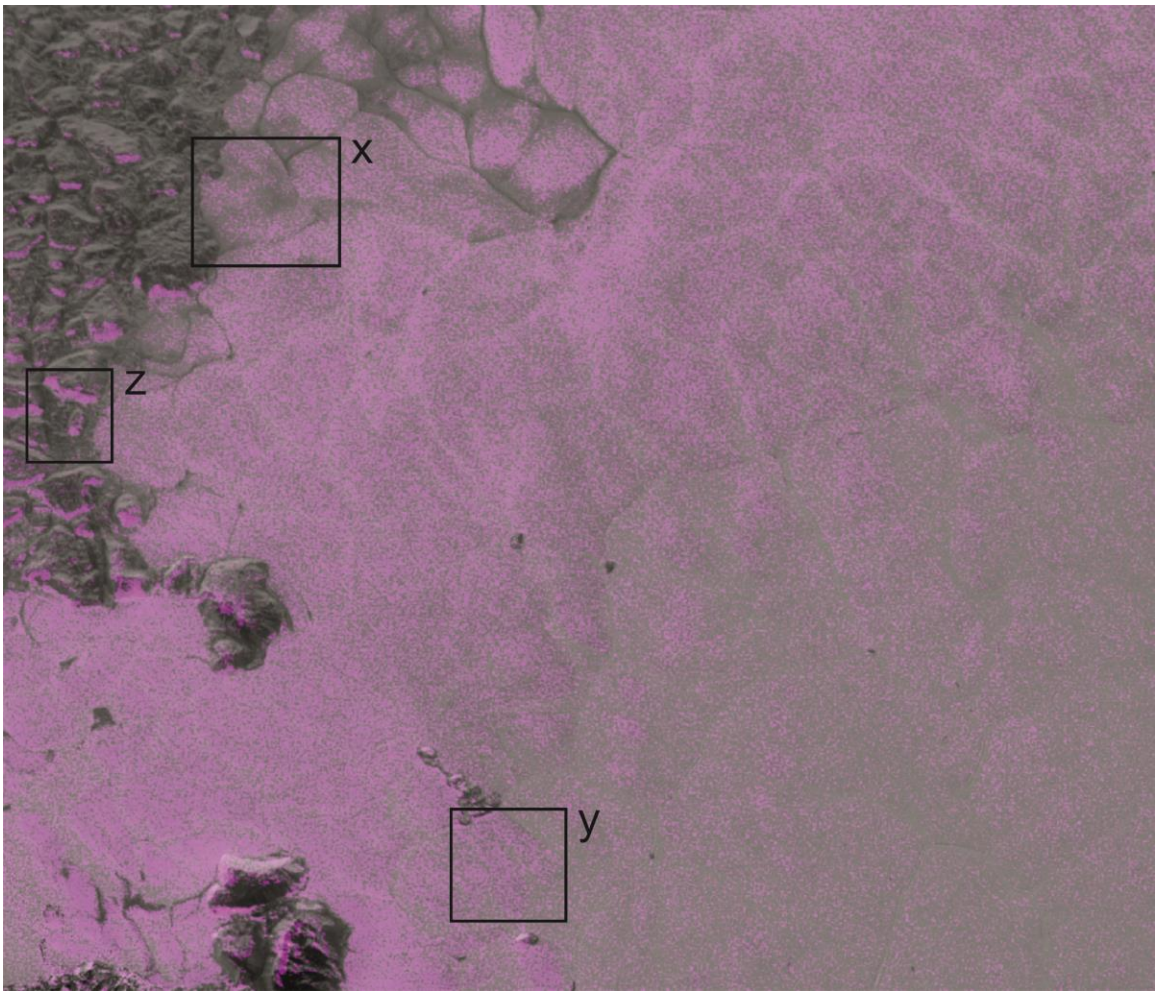


**Fig. S4**

Analysis of MVIC data using a $CH_4$ filter, based on the 0.89 µm absorption band, reveals that the areas where dunes are well developed also show stronger $CH_4$ absorption (x). The extent of the image is indicated in Fig. S1. In addition, the wind streaks to the southeast of Colleta de Dados Colles (shown in Fig. 1E) are also highlighted as a strong $CH_4$ response (y). The strongest, although spatially isolated and discrete responses, however, are found in the mountains of AIM, and are likely to indicate frosts and thus, perhaps, a source of sediment for the dunes (e.g. z).

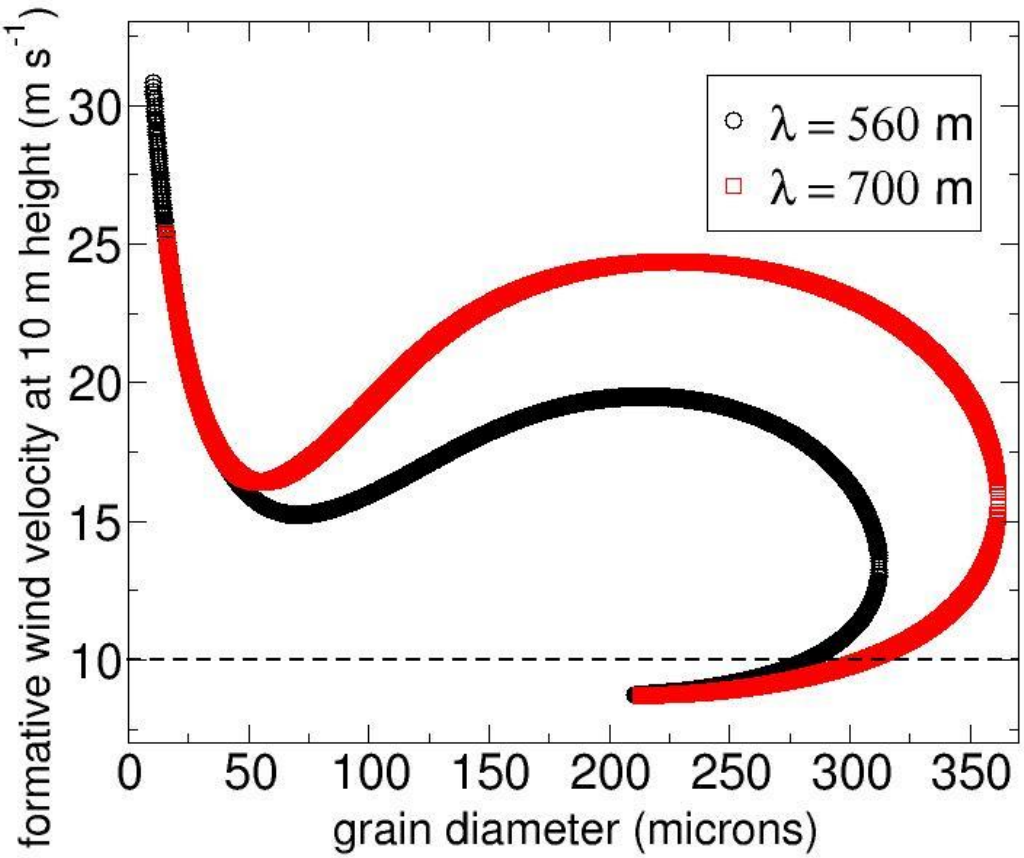


902

903 **Fig. S5.**

904 Possible pairs of grain size and wind velocity (at height of 10 m), which form transverse dunes
905 with the observed values of spacing λ = 560 m and λ= 700 m under the atmospheric conditions
906 valid for Pluto (*15*). The dashed line represents likely maximum wind speeds for Pluto (*16*).

907

908

909

910